

WASP-64 b and WASP-72 b: two new transiting highly irradiated giant planets[★]

M. Gillon¹, D. R. Anderson², A. Collier-Cameron³, A. P. Doyle², A. Fumel¹, C. Hellier², E. Jehin¹, M. Lendl⁴, P. F. L. Maxted², J. Montalbán¹, F. Pepe⁴, D. Pollacco⁵, D. Queloz⁴, D. Ségransan⁴, A. M. S. Smith², B. Smalley², J. Southworth², A. H. M. J. Triaud⁴, S. Udry⁴, R. G. West⁶

¹ Institut d'Astrophysique et de Géophysique, Université de Liège, Allée du 6 août 17, Sart Tilman, Liège 1, Belgium

² Astrophysics Group, Keele University, Staffordshire, ST5 5BG, United Kingdom

³ School of Physics and Astronomy, University of St. Andrews, North Haugh, Fife, KY16 9SS, UK

⁴ Observatoire de Genève, Université de Genève, 51 Chemin des Maillettes, 1290 Sauverny, Switzerland

⁵ Department of Physics, University of Warwick, Coventry CV4 7AL, UK

⁶ Department of Physics and Astronomy, University of Leicester, Leicester, LE1 7RH, UK

Received date / accepted date

ABSTRACT

We report the discovery by the WASP transit survey of two new highly irradiated giant planets transiting moderately bright stars. WASP-64 b is slightly more massive ($1.271 \pm 0.068 M_{Jup}$) and larger ($1.271 \pm 0.039 R_{Jup}$) than Jupiter, and is in very-short ($a = 0.02648 \pm 0.00024$ AU) circular orbit around a $V=12.3$ G7-type dwarf ($1.004 \pm 0.028 M_{\odot}$, $1.058 \pm 0.025 R_{\odot}$, $T_{eff} = 5500 \pm 150$ K). Its size is typical of hot Jupiters with similar masses. WASP-72 b has also a mass a bit larger than Jupiter's ($1.410^{+0.045}_{-0.050} M_{Jup}$) and orbits very close ($0.03655^{+0.00039}_{-0.00032}$ AU) to a slightly evolved $V=9.6$ F7-type star ($1.327^{+0.043}_{-0.035} M_{\odot}$, $1.71^{+0.16}_{-0.09} R_{\odot}$, $T_{eff} = 6250 \pm 100$ K). Despite its extreme irradiation ($\sim 4 \times 10^9$ erg s⁻¹ cm⁻²), WASP-72 b has a size consistent with Jupiter's ($1.01^{+0.12}_{-0.08} R_{Jup}$) that makes it a possible outlier among the hot Jupiters of similar masses, suggesting a significant enrichment in heavy elements.

Key words. stars: planetary systems - star: individual: WASP-64 - star: individual: WASP-72 - techniques: photometric - techniques: radial velocities - techniques: spectroscopic

1. Introduction

The booming study of exoplanets allow us to assess the diversity of the planetary systems of the Milky Way and to put our own solar system in perspective. Notably, ground-based transit surveys targeting relatively bright ($V < 13$) stars are detecting at an increasing rate short-period giant planets amenable for a thorough characterization (orbit, structure, atmosphere), thanks to the brightness of their host star, the favorable planet-star size ratio and their large stellar irradiation (e.g. Winn 2010). With its very high detection efficiency, the WASP transit survey (Pollacco et al. 2006) is one of the most productive projects in that domain.

In this context, we report here the detection by WASP of two new giant planets, WASP-64 b and WASP-72 b, transiting relatively bright Southern stars. Section 2 presents the WASP discovery photometry, and high-precision follow-up observations obtained from La Silla ESO Observatory (Chile) by the TRAPPIST and *Euler* telescopes to confirm the transits and planetary nature of both objects and to determine precisely the systems parameters. In Sect. 3, we present the spectroscopic determination of the stellar properties and the derivation of the system parameters through a combined analysis of the follow-up photometric and spectroscopic time-series. Finally, we discuss our results in Sect. 4.

Send offprint requests to: michael.gillon@ulg.ac.be

[★] The photometric time-series used in this work are only available in electronic form at the CDS via anonymous ftp to cdsarc.u-strasbg.fr (130.79.128.5) or via <http://cdsweb.u-strasbg.fr/cgi-bin/qcat?J/A+A/>

2. Observations

2.1. WASP transit detection photometry

The stars 1SWASPJ064427.63-325130.4 (WASP-64; $V=12.3$, $K=11.0$) and 1SWASPJ024409.60-301008.5 (WASP-72; $V=10.1$, $K=9.6$) were observed by the Southern station of the WASP survey (Hellier et al. 2011) between 2006 Oct 11 and 2010 Mar 12 and between 2006 Aug 11 and 2007 Dec 31, respectively. The 17912 and 6500 pipeline-processed photometric measurements were detrended and searched for transits using the methods described by Collier-Cameron et al. (2006). The selection process (Collier-Cameron et al. 2007) identified WASP-72 as a high priority candidate showing periodic low-amplitude (2-3 mmag) transit-like signatures with period of 2.217 days. For WASP-64, similar transit-like signals with a period of 1.573 days were also detected, still not on WASP-64 itself but on a brighter star at $28''$, 1SWASPJ064429.53-325129.5 (TYC7091-1288-1, $V=12.3$, $K=11.0$). Fig. 1 presents for TYC7091-1288-1 and WASP-72 the WASP photometry folded on the deduced transit ephemeris.

A search for periodic modulation was applied on the photometry of WASP-72, using for this purpose the method described in Maxted et al. (2011). No periodic signal was found down to the mmag amplitude. We did not perform such a search for TYC7091-1288-1, as it is blended with other stars at the spatial resolution of the WASP instrument (see below).

2.2. Follow-up photometry

2.2.1. WASP-64

WASP-64 is at 28" West from TYC7091-1288-1, close enough to have most of its point-spread function (PSF) enclosed in the smallest of the WASP photometry extraction apertures (radius=34", see Fig. 2). It was thus evenly possible that the eclipse signal detected by WASP was originating from one or the other star, so our first follow-up action was to measure on 2011 Jan 20 a transit at a better spatial resolution with the robotic 60cm telescope TRAPPIST (*TR*Ansiting *Pl*anets and *Pl*anetes/*Im*als Small Telescope; Gillon et al. 2011, Jehin et al. 2011) located at ESO La Silla Observatory in the Atacama Desert, Chile. TRAPPIST is equipped with a thermoelectrically-cooled 2K × 2K CCD having a pixel scale of 0.65" that translates into a 22' × 22' field of view. Differential photometry was obtained with TRAPPIST for both stars on the night of 2011 Jan 20, corresponding to a transit window as derived from WASP data. These observations were obtained with the telescope focused and through a special '*I* + *z*' filter that has a transmittance >90% from 750 nm to beyond 1100 nm¹. The positions of the stars on the chip were maintained to within a few pixels over the course of the run, thanks to a 'software guiding' system deriving regularly an astrometric solution for the most recently acquired image and sending pointing corrections to the mount if needed. After a standard pre-reduction (bias, dark, flatfield correction), the stellar fluxes were extracted from the images using the IRAF/DAOPHOT² aperture photometry software (Stetson, 1987). Several sets of reduction parameters were tested, and we kept the one giving the most precise photometry for the stars of similar brightness as the target. After a careful selection of reference stars, differential photometry was then obtained. This reduction procedure was also applied for the subsequent TRAPPIST runs.

This first TRAPPIST run resulted in a flat light curve for TYC7091-1288-1, while the light curve for WASP-64 showed a clear transit-like structure (Fig. 2), identifying thus WASP-64 as the source of the transit signal. A second (partial) transit was observed in the *I* + *z* filter on 2011 Feb 22 to better constrain the shape of the eclipse (Fig. 3, second light curve from the top). As for the following WASP-64 transits, the telescope was defocused to ~3" to improve the duty cycle and average the pixel-to-pixel effects. A global analysis of the two first TRAPPIST transit light curves led to an eclipse depth and shape compatible with the transit of a giant planet in front of a solar-type star. Our next action was to observe a third transit with TRAPPIST, this time in the *V* filter to assess the chromaticity of the transit depth (Fig. 3, third light curve from the top). The analysis of the resulting light curve led to a transit depth consistent with the one measured in the *I* + *z* filter, as expected for a transiting planet. We then observed an *occultation* window in the *z'*-band on 2011 Apr 30. We could not detect any eclipse in the resulting photometric time-series (Fig. 4), which was again consistent with the transiting planet scenario. At this stage, we began our spectroscopic follow-up of WASP-64 that confirmed the solar-type nature of WASP-64 and the planetary nature of its eclipsing companion (see Sec. 2.3).

Once the planetary nature of WASP-64 b confirmed, we observed seven more of its transits with TRAPPIST, using then a

blue-blocking filter³ that has a transmittance >90% from 500 nm to beyond 1000 nm. The goal of using this very wide red filter is to maximize the signal-to-noise ratio (SNR) while minimizing the influence of moonlight pollution, differential extinction and stellar limb-darkening on the transit light curves. The resulting light curves are shown in Fig. 3 (fifth to last light curves from the top). The transit of 2011 Oct 19 was also observed in the Gunn-*r* filter with the EulerCam CCD camera at the 1.2-m *Euler* Telescope at La Silla Observatory. This nitrogen-cooled camera has a 4k × 4k E2V CCD with a 15' × 15' field of view (scale=0.23"/pixel). Here too, a defocus was applied to the telescope to optimize the observation efficiency and minimize pixel-to-pixel effects, while flatfield effects were further reduced by keeping the stars on the same pixels, thanks to a 'software guiding' system similar to the one of TRAPPIST (Lendl et al. 2012). The reduction was similar to that performed on TRAPPIST data. The resulting light curve is also shown in Fig. 3 (fourth light curve from the top).

2.2.2. WASP-72

We monitored for WASP-72 three transits with TRAPPIST (see Table 1 and Fig. 5), two partial transits in the *I* + *z* filter and one full transit in the blue-blocking filter. For the three transits, the telescope was defocused to ~3". A first partial transit was observed in 2011 Jan 21 in the *I* + *z* filter at high airmass, confirming the low-amplitude eclipse detected by WASP (Fig. 5, first light curve from the top). The next season, a full transit was observed on 2011 Oct 25 in the blue-blocking filter. A technical problem damaged these data: a shutter problem led to a scatter twice larger than expected (Fig. 5, fourth light curve from the top). Finally, a partial transit was observed in the *I* + *z* filter on 2011 Dec 4 (Fig 5, second light curve from the top). A transit of WASP-72 was also observed with *Euler* on 2011 Nov 25-26 night, with the same strategy than for WASP-64 (Fig. 5, third light curve from the top).

Table 1 presents a summary of the follow-up photometric time-series obtained for WASP-64 and WASP-72.

2.3. Spectroscopy and radial velocities

Once WASP-64 and WASP-72 were identified as high priority candidates, we gathered spectroscopic measurements with the CORALIE spectrograph mounted on *Euler* to confirm the planetary nature of the eclipsing bodies and obtain mass measurements. 16 usable spectra were obtained for WASP-64 from 2011 May 2 to 2011 November 7 with an exposure time of 30 minutes. For WASP-72, 18 spectra were gathered from 2011 January 9 to 2011 December 29, here too with an exposure time of 30 minutes. Radial velocities (RVs) were computed by weighted cross-correlation (Baranne et al. 1996) with a numerical G2-spectral template for both stars and are shown in Table 2.

The RV time-series show variations that are consistent with planetary-mass companions. Preliminary orbital analyses of the RVs resulted in periods and phases in excellent agreement with those deduced from the WASP transit detections (Fig. 6 & 7, upper panels). For WASP-64, assuming a stellar mass $M_* = 0.98 \pm 0.09 M_\odot$ (Sect. 3.1), the fitted semi-amplitude $K = 212 \pm 17 \text{ m s}^{-1}$ translates into a secondary mass slightly larger than Jupiter's, $M_p = 1.19 \pm 0.12 M_{\text{Jup}}$. The resulting orbital eccentricity is consistent with zero, $e = 0.05^{+0.06}_{-0.03}$. For WASP-72,

³ <http://www.astrodon.com/products/filters/exoplanet/>

¹ <http://www.astrodon.com/products/filters/near-infrared/>

² IRAF is distributed by the National Optical Astronomy Observatory, which is operated by the Association of Universities for Research in Astronomy, Inc., under cooperative agreement with the National Science Foundation.

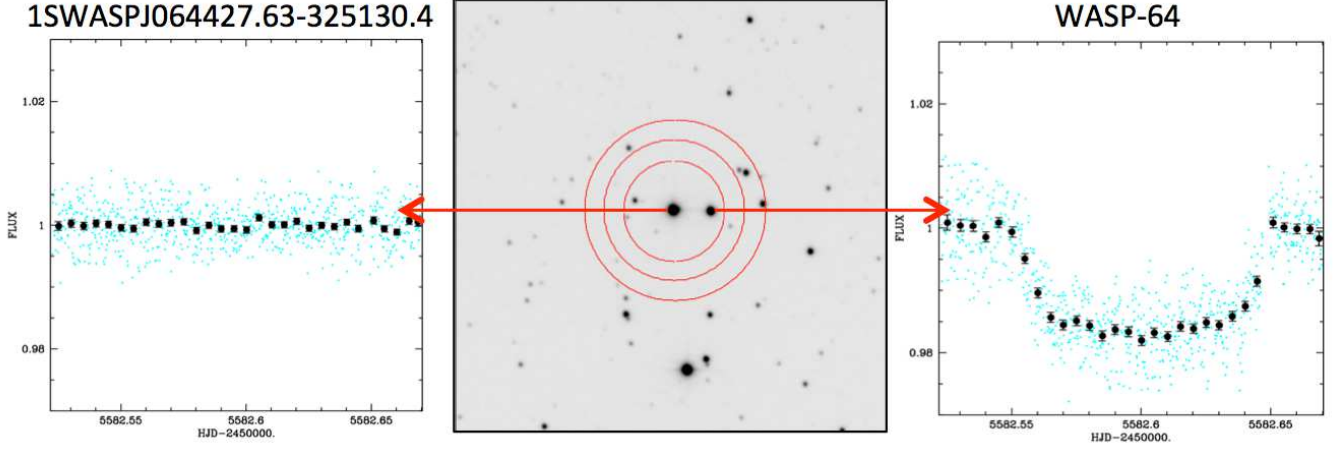


Fig. 2. 280'' \times 280'' TRAPPIST $I + z$ image centered on TYC7091-1288-1. North is up and East is left. The three concentric circles indicate the three photometry extraction apertures used in the WASP pipeline. WASP-64 is the closest star to the right of TYC7091-1288-1. For both stars, the light curve obtained by TRAPPIST on 2011 Jan 20 is shown (cyan=unbinned, black=binned per intervals of 0.005d).

Target	Night	Telescope	Filter	N	T_{exp} (s)	Baseline function	Eclipse nature
WASP-64	2011 Jan 20-21	TRAPPIST	$I + z$	792	8	$p(t^2) + o$	transit
WASP-64	2011 Feb 22-23	TRAPPIST	$I + z$	296	20	$p(t^2)$	transit
WASP-64	2011 Apr 4-5	TRAPPIST	V	364	30	$p(t^2)$	transit
WASP-64	2011 Apr 30 - May 1	TRAPPIST	z'	202	40	$p(t^2)$	occultation
WASP-64	2011 Oct 19-20	TRAPPIST	BB	578	15	$p(t^2)$	transit
WASP-64	2011 Oct 19-20	<i>Euler</i>	Gunn- r	159	60	$p(t^2)$	transit
WASP-64	2011 Oct 30-31	TRAPPIST	BB	533	15	$p(t^2)$	transit
WASP-64	2011 Nov 21-22	TRAPPIST	BB	512	15	$p(t^2) + o$	transit
WASP-64	2011 Nov 29-30	TRAPPIST	BB	611	15	$p(t^2)$	transit
WASP-64	2011 Dec 10-11	TRAPPIST	BB	642	15	$p(t^2) + o$	transit
WASP-64	2011 Dec 21-22	TRAPPIST	BB	566	15	$p(t^2) + o$	transit
WASP-64	2012 Jan 12-13	TRAPPIST	BB	578	15	$p(t^2)$	transit
WASP-72	2011 Jan 21-22	TRAPPIST	$I + z$	707	8	$p(t^2)$	transit
WASP-72	2011 Oct 25-26	TRAPPIST	BB	2042	4	$p(t^2) + o$	transit
WASP-72	2011 Nov 25-26	<i>Euler</i>	Gunn- r	294	40	$p(t^2) + p(a^2)$	transit
WASP-72	2011 Dec 4-5	TRAPPIST	$I + z$	892	10	$p(t^2) + o$	transit

Table 1. Summary of follow-up photometry obtained for WASP-64 and WASP-72. N = number of measurements. T_{exp} = exposure time. BB = blue-blocking filter. The baseline functions are the analytical functions used to model the photometric baseline of each light curve (see Sec. 3.2). $p(t^2)$ denotes a quadratic time polynomial, $p(a^2)$ a quadratic airmass polynomial, and o an offset fixed at the time of the meridian flip.

assuming a stellar mass $M_* = 1.23 \pm 0.10 M_{\odot}$ (Sect. 3.1), the fitted semi-amplitude $K = 179 \pm 6 \text{ m s}^{-1}$ translates into a secondary mass $M_p = 1.31 \pm 0.08 M_{\text{Jup}}$, while the deduced orbital eccentricity is also consistent with zero, $e = 0.05^{+0.03}_{-0.03}$.

A model with a slope is slightly favored in the case of WASP-72, its value being $-82 \pm 22 \text{ m s}^{-1}$ per year. Indeed, the respective values for the Bayesian Information Criterion (BIC; Schwarz 1978) led to likelihood ratios (Bayes factors) between 10 and 55 in favor of the slope model, depending if the orbit was assumed to be circular or not. Such values for the Bayes factor are not large enough to be decisive, and more RVs will be needed to confirm this possible trend.

To exclude the possibility that the RV signal originates from spectral line distortions caused by a blended eclipsing binary, we analyzed the CORALIE cross-correlation functions (CCF) using the line-bisector technique described in Queloz et al (2001). The bisector spans revealed to be stable, their standard deviation being close to their average error (57 vs 47 m s^{-1} for WASP-64 and 28 vs 24 m s^{-1} for WASP-72). No evidence for a correlation between the RVs and the bisector spans was found (Fig. 6 & 7, lower panels), the deduced correlation coefficients being -0.04 (WASP-64) and 0.06 (WASP-72). We concluded thus that the stars WASP-64 and WASP-72 are transited by a giant planet every ~ 1.573 and ~ 2.217 days, respectively.

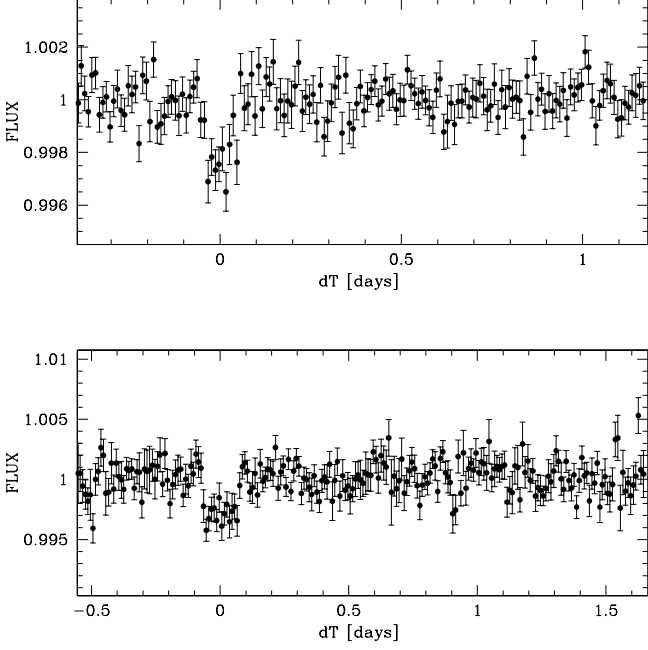


Fig. 1. WASP photometry for TYC7091-1288-1 (*top*) and WASP-72 (*bottom*) folded on the best-fitting transit ephemeris from the transit search algorithm presented in Collier Cameron et al. (2006), and binned per 0.01d intervals

3. Analysis

3.1. Spectroscopic analysis - stellar properties

The CORALIE spectra of WASP-64 and WASP-72 were co-added to produce single spectra with average SNR of 60 and 80, respectively. The standard pipeline reduction products were used in the analysis.

The spectral analysis was performed using the methods given by Gillon et al. (2009a). The H_α line was used to determine the effective temperature (T_{eff}). For WASP-64, the Na I D and Mg I b lines were used as surface gravity ($\log g$) diagnostics, while for WASP-72, $\log g$ was determined from the Ca I lines at 6162Å and 6439Å (Bruntt et al. 2010a), along with the Na I D lines. The parameters obtained from the analysis are listed in Table 3. The elemental abundances were determined from equivalent width measurements of several clean and unblended lines. A value for microturbulence (ξ_t) was determined from Fe I lines using the method of Magain (1984). The quoted error estimates include those given by the uncertainties in T_{eff} , $\log g$ and ξ_t , as well as the scatter due to measurement and atomic data uncertainties.

The projected stellar rotation velocities ($v \sin i_*$) were determined by fitting the profiles of several unblended Fe I lines. Values for macroturbulence (v_{mac}) of 1.8 ± 0.3 and 4.0 ± 0.3 km s^{-1} were assumed for WASP-64 and WASP-72, respectively, based on the calibration by Bruntt et al. (2010b). An instrumental FWHM of 0.11 ± 0.01 Å was determined for both stars from the telluric lines around 6300Å. Best-fitting values of $v \sin i_* = 3.4 \pm 0.8$ km s^{-1} (WASP-64) and $v \sin i_* = 6.0 \pm 0.7$ km s^{-1} (WASP-72) were obtained.

There is no significant detection of lithium in the spectra, with equivalent width upper limits of 2mÅ for both stars, corresponding to abundance upper limits of $\log A(\text{Li}) < 0.61 \pm 0.15$

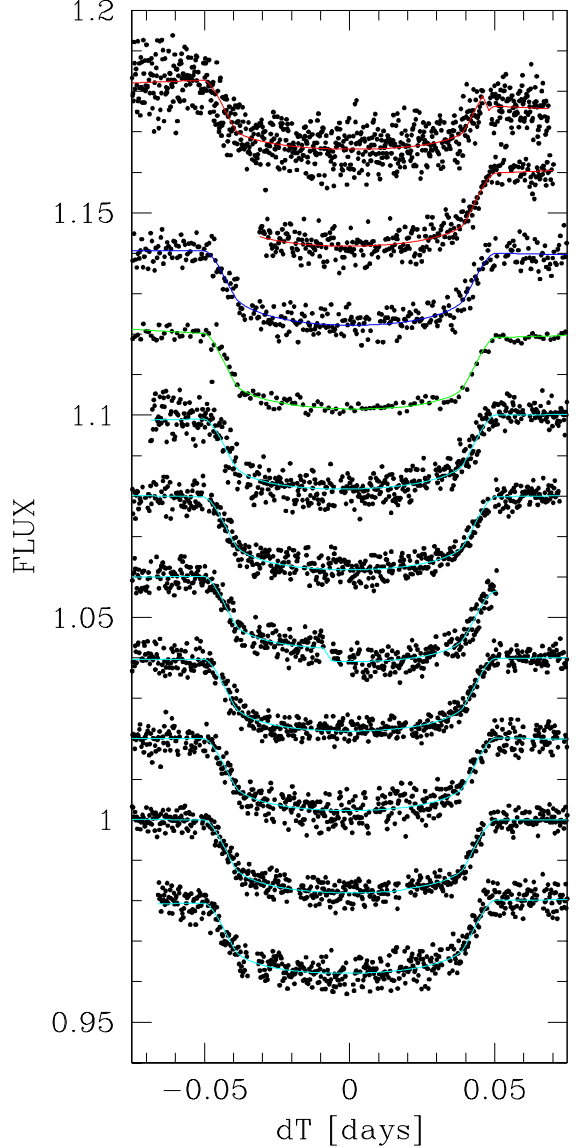


Fig. 3. Follow-up transit photometry for WASP-64. From top to bottom are TRAPPIST $I + z$ filter (1, 2), TRAPPIST V filter (3), Euler Gunn- r filter (4), and TRAPPIST blue-blocking filter (5 to 11). For each light curve, the best-fit transit+baseline model deduced from the global analysis is superimposed (see Sec. 3.2). The light curves are shifted along the y-axis for clarity.

(WASP-64) and $\log A(\text{Li}) < 1.21 \pm 0.17$ (WASP-72). These imply ages of at least a few Gyr (Sestito & Randich, 2005).

The rotation rate for WASP-64 ($P_{\text{rot}} = 15.3 \pm 4.7$ d) and WASP-72 ($P_{\text{rot}} = 11.6 \pm 2.7$ d) implied by the $v \sin i_*$ give gyrochronological ages of $\sim 1.2^{+1.2}_{-0.7}$ Gyr (WASP-64) and $\sim 2.4^{+2.8}_{-1.3}$ Gyr (WASP-72) under the Barnes (2007) relation.

We obtained with CORALIE two spectra of TYC7091-1288-1, the brighter star lying at 28" East from WASP-64 (Sec. 2.2.1, Fig. 2). The co-added spectrum has a SNR of only ~ 30 . A spectral analysis led to $T_{\text{eff}} \sim 5700$ K and $\log g \sim 4.5$, with no sign of any significant lithium absorption, and a low $v \sin i_* \sim 4$ km s^{-1} . The RV is ~ 35 km s^{-1} , compared to 33.2 km s^{-1} for WASP-64.

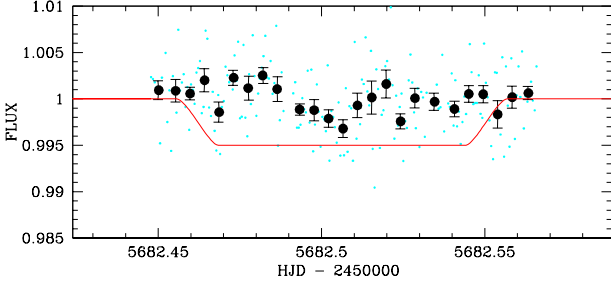


Fig. 4. TRAPPIST z' time-series photometry obtained during an occultation window of WASP-64 b, unbinned and binned per intervals of 0.005d. An occultation model assuming a circular orbit and a depth of 0.5% is superimposed for comparison.

Target	$HJD_{TDB}-2450000$	RV (km s^{-1})	σ_{RV} (m s^{-1})	BS (km s^{-1})
WASP-64	5622.652685	33.1075	21.5	0.1171
WASP-64	5629.582507	33.3234	19.8	-0.0900
WASP-64	5681.541466	33.3368	23.9	-0.0601
WASP-64	5696.488635	33.0326	24.3	-0.0057
WASP-64	5706.460152	33.4079	24.3	-0.0156
WASP-64	5707.460947	33.0038	28.0	-0.0075
WASP-64	5708.461813	33.2129	25.1	-0.0169
WASP-64	5711.463695	33.3160	26.3	0.0040
WASP-64	5715.458133	33.1019	27.2	-0.0645
WASP-64	5716.463634	33.0977	26.1	-0.0121
WASP-64	5842.867334	33.0986	24.0	-0.0453
WASP-64	5861.847564	33.1559	25.4	0.0061
WASP-64	5864.795499	33.0230	18.1	-0.0346
WASP-64	5869.724123	33.1725	20.6	-0.0504
WASP-64	5871.734734	33.4248	21.1	0.0752
WASP-64	5872.762875	33.1044	20.1	0.0877
WASP-72	5570.618144	35.7945	13.3	0.0176
WASP-72	5828.890931	36.0233	11.3	0.0566
WASP-72	5829.865219	35.8029	9.8	0.0466
WASP-72	5830.866138	35.9320	11.5	0.0623
WASP-72	5832.894502	35.8391	14.6	0.0396
WASP-72	5852.780149	35.7640	15.5	0.0092
WASP-72	5856.757447	35.7288	11.5	0.0390
WASP-72	5858.689011	35.8146	15.2	-0.0198
WASP-72	5863.800340	35.7664	10.4	0.0462
WASP-72	5864.750293	36.0695	10.0	0.0292
WASP-72	5865.812141	35.7283	11.9	0.0968
WASP-72	5866.605265	36.0331	10.6	0.0734
WASP-72	5867.628720	35.7586	10.3	0.0605
WASP-72	5868.759336	35.9966	10.4	-0.0019
WASP-72	5873.808914	35.9928	10.9	0.0368
WASP-72	5886.748911	36.0460	16.3	0.0624
WASP-72	5914.700813	35.7261	9.5	0.0504
WASP-72	5924.584434	36.0624	10.0	0.0562

Table 2. CORALIE radial-velocity measurements for WASP-64 and WASP-72 (BS = bisector spans).

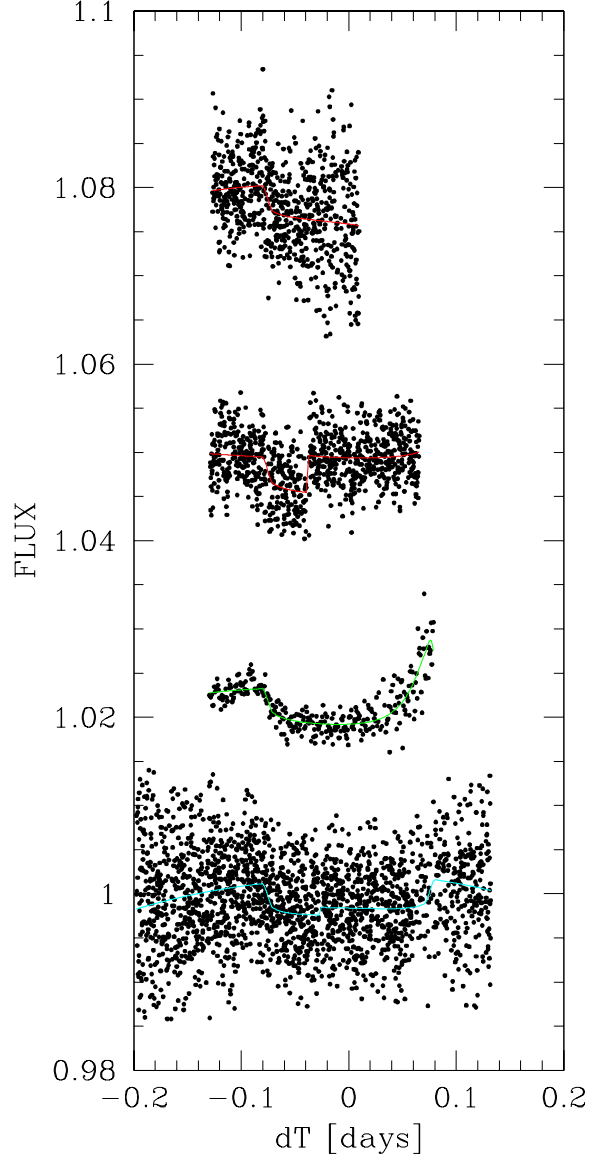


Fig. 5. Follow-up transit photometry for WASP-72. From top to bottom are TRAPPIST $I + z$ filter (1, 2), *Euler Gunn-r* filter (3), and TRAPPIST blue-blocking filter (4). For each light curve, the best-fit transit+baseline model deduced from the global analysis is superimposed (see Sec. 3.2). The light curves are shifted along the y-axis for clarity. The large jump visible after the ingress in the second TRAPPIST light curve is due to a meridian flip and to the resulting field rotation that put the stars on other pixels. It is modeled as an offset fixed at the time of the meridian crossing.

The cross-correlation function reveals that TYC 7091-1288-1 is an SB2 system (Fig. 8). The PPMXL catalogue (Roeder et al. 2010) shows that proper motions of both stars are consistent to within their quoted uncertainties. If these stars are physically associate, as suggested by their similar proper motions and radial velocities, their angular separation corresponds to a projected distance of 9800 ± 2500 AU, which is possible for a very wide triple system.

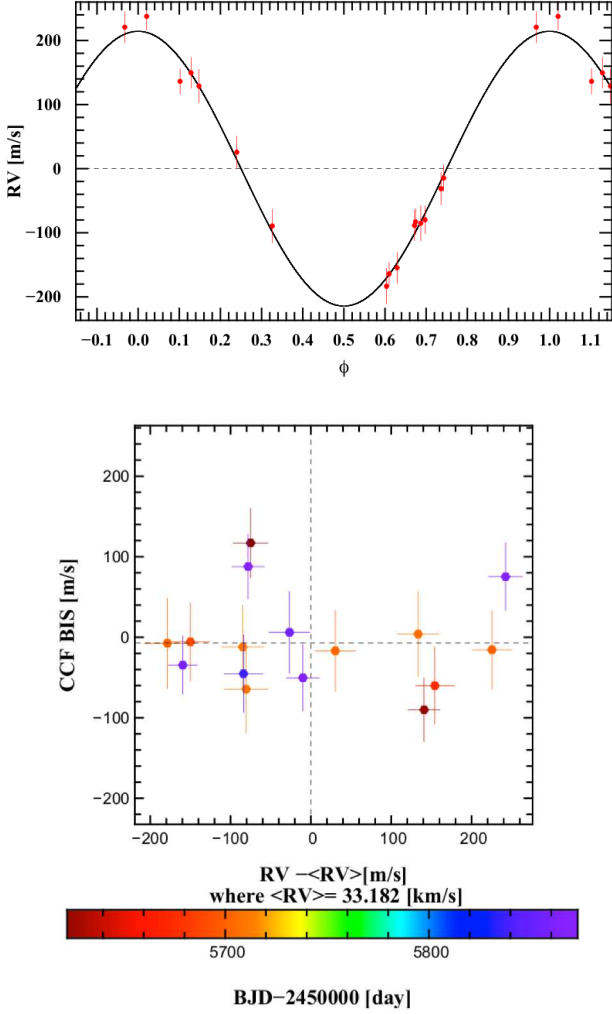


Fig. 6. *Top:* CORALIE RVs for WASP-64 phase-folded on the best-fit orbital period, and with the best-fit Keplerian model over-imposed. *Bottom:* correlation diagram CCF bisector spans vs RV. The colors indicate the measurement timings.

3.2. Global analysis

For both systems, we performed a global analysis of the follow-up photometry and the CORALIE RV measurements. The analysis was performed using the adaptive Markov Chain Monte-Carlo (MCMC) algorithm described by Gillon et al. (2012, and references therein). To summarize, we simultaneously fitted the data, using for the photometry the transit model of Mandel & Agol (2002) multiplied by a baseline model consisting of a different second-order time polynomial for each of the light curves. For six TRAPPIST light curves (see Table 1), a normalization offset was also part of the model to represent the effect of the meridian flip. TRAPPIST’s mount is indeed a german equatorial type, which means that the telescope has to undergo a 180° rotation when the meridian is reached, resulting in different locations of the stellar images on the detector before and after the flip, and thus in a possible jump of the differential flux at the time of the flip. For the WASP-72 *Euler* transit, a quadratic function of airmass had to be added to the baseline model to account for the strong extinction effect caused by the high airmass (>2.5) at the end of the run. On their side, the RVs were modeled with Keplerian orbits, plus a linear trend for WASP-72 (see Sec. 2.3).

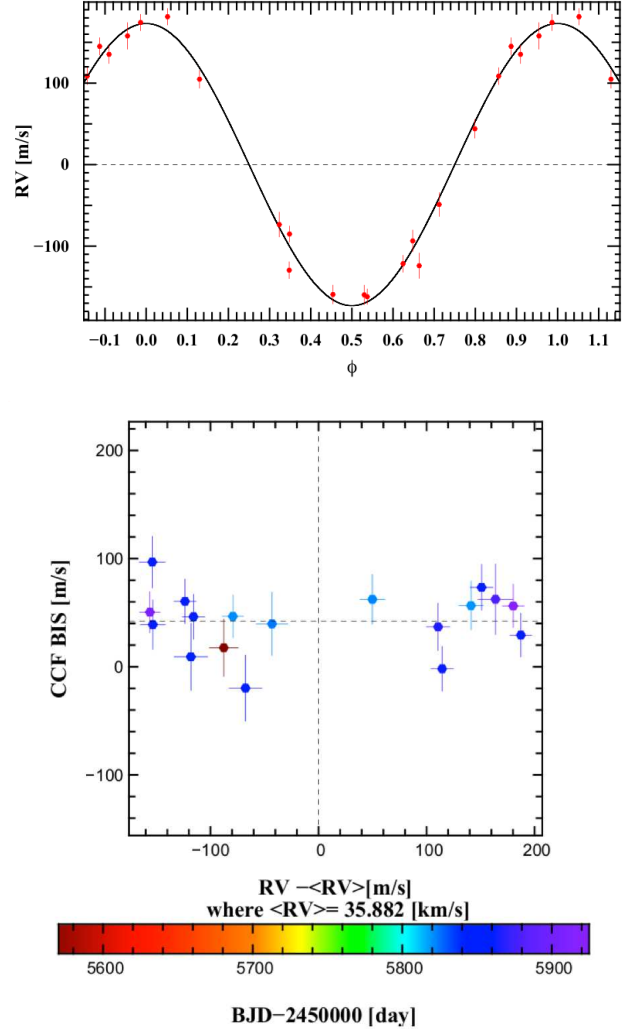


Fig. 7. *Top:* CORALIE RVs for WASP-72 phase-folded on the best-fit orbital period, and with the best-fit Keplerian model over-imposed. *Bottom:* correlation diagram CCF bisector spans vs RV. The colors indicate the measurement timings.

The jump parameters⁴ in our MCMC analysis were: the planet/star area ratio $(R_p/R_*)^2$, the transit width (from first to last contact) W , the parameter $b' = a \cos i_p / R_*$ (which is the transit impact parameter in case of a circular orbit) where a is the planet’s semi-major axis and i_p its orbital inclination, the orbital period P and time of minimum light T_0 , the two parameters $\sqrt{e} \cos \omega$ and $\sqrt{e} \sin \omega$ where e is the orbital eccentricity and ω is the argument of periastron, and the parameter $K_2 = K \sqrt{1 - e^2} P^{1/3}$, where K is the RV orbital semi-amplitude. We assumed a uniform prior distribution for all these jump parameters. The photometric baseline model parameters and the systemic radial velocity of the star γ (and the slope of the trend for WASP-72) were not actual jump parameters, they were determined by least-square minimization at each step of the MCMC.

We assumed a quadratic limb-darkening law, and we allowed the quadratic coefficients u_1 and u_2 to float in our MCMC analysis, using as jump parameters not these coefficients themselves but the combinations $c_1 = 2 \times u_1 + u_2$ and $c_2 = u_1 - 2 \times u_2$ to minimize the correlation of the uncertainties (Holman et al. 2006).

⁴ Jump parameters are the parameters that are randomly perturbed at each step of the MCMC.

Parameter	WASP-64	WASP-72
RA (J2000)	06 44 27.61	02 44 09.60
DEC (J2000)	-32 51 30.25	-30 10 08.5
V	12.29	10.88
K	10.98	9.62
T_{eff}	5550 ± 150 K	6250 ± 100 K
$\log g$	4.4 ± 0.15	4.25 ± 0.15
ξ_t	0.9 ± 0.1 km s $^{-1}$	1.6 ± 0.1 km s $^{-1}$
$v \sin i_*$	3.4 ± 0.8 km s $^{-1}$	6.0 ± 0.7 km s $^{-1}$
[Fe/H]	-0.08 ± 0.11	-0.06 ± 0.09
[Na/H]	0.14 ± 0.08	-0.03 ± 0.04
[Mg/H]	0.12 ± 0.12	
[Al/H]	0.00 ± 0.08	
[Si/H]	0.10 ± 0.10	0.02 ± 0.07
[Ca/H]	0.05 ± 0.16	0.07 ± 0.14
[Sc/H]	0.07 ± 0.10	0.14 ± 0.07
[Ti/H]	-0.02 ± 0.11	0.07 ± 0.11
[V/H]	0.03 ± 0.16	-0.01 ± 0.08
[Cr/H]	0.01 ± 0.08	0.02 ± 0.10
[Mn/H]	0.09 ± 0.10	-0.11 ± 0.06
[Co/H]	0.06 ± 0.09	-0.06 ± 0.18
[Ni/H]	-0.04 ± 0.11	-0.04 ± 0.06
$\log A(\text{Li})$	$< 0.61 \pm 0.15$	$< 1.21 \pm 0.17$
Mass	$0.98 \pm 0.09 M_{\odot}$	$1.23 \pm 0.10 M_{\odot}$
Radius	$1.03 \pm 0.20 R_{\odot}$	$1.37 \pm 0.27 R_{\odot}$
Sp. Type	G7	F7
Distance	350 ± 90 pc	250 ± 30 pc

Table 3. Basic and spectroscopic parameters of WASP-64 and WASP-72 from spectroscopic analysis.

Note: Mass and Radius estimate using the calibration of Torres et al. (2010). Spectral type estimated from T_{eff} using the table in Gray (2008).

Limb-darkening coefficient	WASP-64	WASP-72
$u1_V$	0.50 ± 0.035	-
$u2_V$	0.23 ± 0.025	-
$u1_{\text{Gunn-r}}$	0.43 ± 0.03	0.31 ± 0.015
$u2_{\text{Gunn-r}}$	0.26 ± 0.02	0.315 ± 0.005
$u1_{BB}$	0.36 ± 0.05	0.255 ± 0.04
$u2_{BB}$	0.255 ± 0.02	0.305 ± 0.01
$u1_{I+z}$	0.29 ± 0.03	0.205 ± 0.02
$u2_{I+z}$	0.255 ± 0.015	0.295 ± 0.01

Table 4. Expectation and standard deviation of the normal distributions used as prior distributions for the quadratic limb-darkening coefficients $u1$ and $u2$ in our MCMC analysis.

To obtain a limb-darkening solution consistent with theory, we used normal prior distributions for u_1 and u_2 based on theoretical values and $1\text{-}\sigma$ errors interpolated in the tables by Claret (2000; 2004) and shown in Table 4. For our two non-standard filters ($I+z$ and blue-blocking), we estimated the effective wavelength basing on the transmission curves of the filters, the quantum efficiency curve of the camera and the spectral energy distributions of the stars (assumed to emit as blackbodies), and we interpolated the corresponding limb-darkening coefficient values in Claret’s tables and estimated their errors by using the values for the two nearest standard filters.

Our analysis was composed of five Markov chains of 10^5 steps, the first 20% of each chain being considered as its burn-in phase and discarded. For each run the convergence of the five

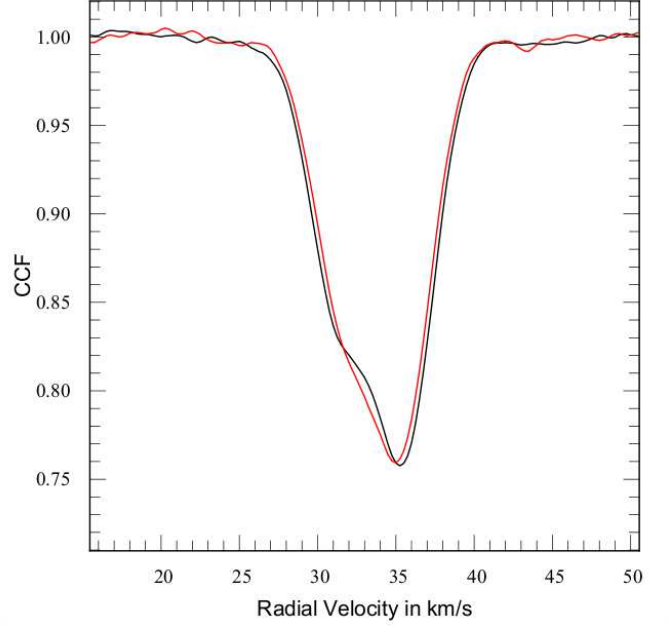


Fig. 8. The cross-correlation functions for the two CORALIE spectra of TYC7091-1288-1. Their clear asymmetry indicates the SB2 nature of the star.

Markov chains was checked using the statistical test presented by Gelman and Rubin (1992). The correlated noise present in the light curves was taken into account as described by Gillon et al. (2009b). For the WASP-72 RVs, a ‘jitter’ noise of 5.1 m s^{-1} was added quadratically to the error bars, to equalize the mean error with the *rms* of the best-fitting model residuals.

At each step of the Markov chains the stellar density ρ_* deduced from the jump parameters, and values for T_{eff} and [Fe/H] drawn from the normal distributions deduced from our spectroscopic analysis (Sect. 3.1), were used to determine a value for the stellar mass M_* through an empirical law $M_*(\rho_*, T_{\text{eff}}, [\text{Fe}/\text{H}])$ (Enoch et al. 2010; Gillon et al. 2011) calibrated using the parameters of the extensive list of stars belonging to detached eclipsing binary systems presented by Southworth (2011). For WASP-64, the list was restricted to the 113 stars with a mass between 0.5 and $1.5 M_{\odot}$, while the 212 stars with a mass between 0.7 to $1.7 M_{\odot}$ were used for WASP-72, the goal of this selection being to benefit from our preliminary estimation of the stellar mass (Sec. 3.1, Table 3) to improve the determination of the physical parameters while using a number of calibration stars large enough to avoid small number statistical effects. To propagate properly the errors on the calibration law, the parameters of the selected subset of eclipsing binary stars were normally perturbed within their observational error bars and the coefficients of the law were redetermined at each MCMC step. Using the resulting stellar mass, the physical parameters of the system were then deduced from the jump parameters.

For both systems, two analyses were performed, one assuming a circular orbit and the other an eccentric orbit. For the sake of completeness, the derived parameters for both models are shown in Table 5 (WASP-64) and Table 6 (WASP-72), while the best-fit transit models are shown in Fig. 9 and 10 for the circular model. Using the BIC as proxy for the model marginal likelihood, the resulting Bayes factors are ~ 3000 (WASP-64) and ~ 5000 (WASP-72) in favor of the circular models. A circular orbit is thus favored for both systems, and we adopt the

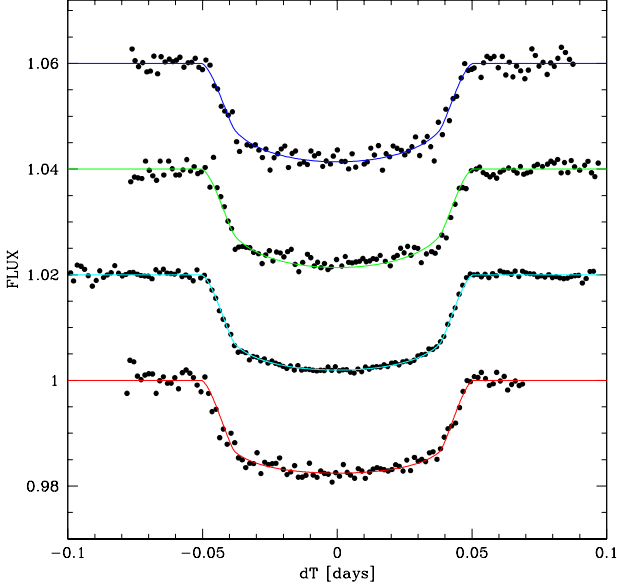


Fig. 9. Combined follow-up transit photometry for WASP-64 b, detrended, period-folded and binned per intervals of 2 min. From top to bottom: *V*, Gunn-*r*, blue-blocking and *I* + *z* filter photometry. For each filter, the best-fit transit model from the global MCMC analysis is superimposed. The *V*, Gunn-*r* and blue-blocking light curves are shifted along the *y*-axis for the sake of clarity.

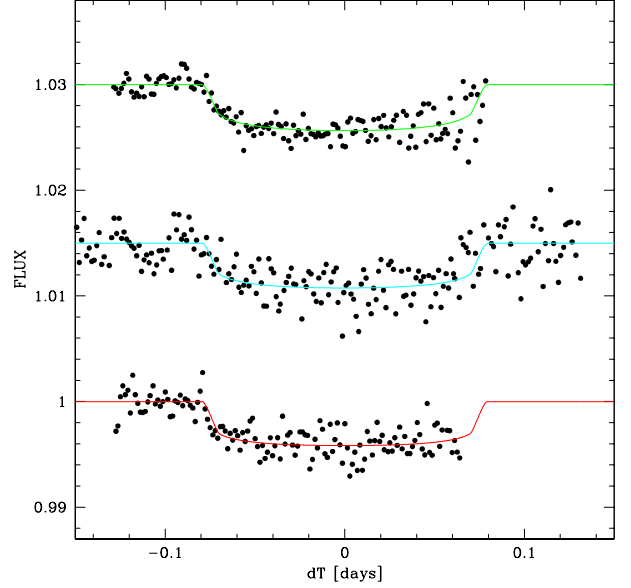


Fig. 10. Combined follow-up transit photometry for WASP-72 b, detrended, period-folded and binned per intervals of 2 min. From top to bottom: Gunn-*r*, blue-blocking and *I* + *z* filter photometry. For each filter, the best-fit transit model from the global MCMC analysis is superimposed. The Gunn-*r* and blue-blocking light curves are shifted along the *y*-axis for the sake of clarity.

corresponding results as our nominal solutions. This choice is strengthened by the modeling of the tidal evolution of both planets, as discussed in Sec. 4.

To assess the reliability of the deduced physical parameters and to estimate their age, we performed for both systems a stellar evolution modeling based on the code CLES (Scuflaire et al. 2008), using as input the stellar densities deduced from the MCMC analyses, and the effective temperatures and metallicities deduced from our spectroscopic analyses. The resulting stellar masses were $0.95 \pm 0.05 M_{\odot}$ (WASP-64) and $1.25 \pm 0.05 M_{\odot}$ (WASP-72), consistent with the MCMC results, while the resulting ages were 7.0 ± 3.5 (WASP-64) and 3.5 ± 0.2 Gy (WASP-72).

3.2.1. Global analysis of the transits with free timings

As a complement to our global analysis, we performed for both systems another global analysis with the timing of each transit being free parameters in the MCMC. The goal here was to benefit from the strong constraint brought on the transit shape provided by the total data set to derive accurate transit timings and to assess the transit periodicity. In this analysis, the parameters T_0 and P were kept under the control of normal prior distributions based on the values shown for a circular orbit in Table 5 (WASP-64) and Table 6 (WASP-72), and we added a timing offset as jump parameter for each transit. The orbits were assumed to be circular. The resulting transit timings and their errors are shown in Table 7. This table also shows (last column) the resulting transit timing variations (TTV = observed minus computed timing, O-C). These TTVs are shown as a function of the transit epochs in Fig. 11. They are all compatible with zero, i.e. there is no sign of transit aperiodicity.

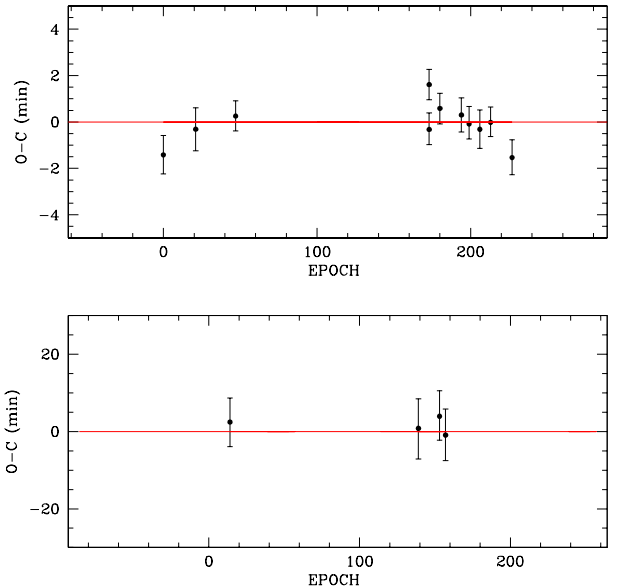


Fig. 11. TTVs ($O - C =$ observed minus computed timing) derived from the global MCMC analyzes of the WASP-64 b (top) and WASP-72 b (bottom) transits (see Sec. 3.2.1).

4. Discussion

WASP-64 b and WASP-72 b are thus two new very short-period (1.57d and 2.22d) planets slightly more massive than Jupiter orbiting moderately bright ($V=12.3$ and 10.1) Southern stars. Their detection demonstrates nicely the high photometric potential of the WASP transit survey (Pollacco et al. 2006), as both planets

Planet	Epoch	Transit timing - 2450000 [HJD_{TDB}]	$O - C$ [s]
WASP-64 b	0	5582.60070 ± 0.00051	-85 ± 50
	21	5615.64057 ± 0.00057	-19 ± 55
	47	5656.54655 ± 0.00035	$+15 \pm 39$
	173	5854.78224 ± 0.00027	$+97 \pm 40$
	173	5854.78091 ± 0.00032	-19 ± 41
	180	5865.79456 ± 0.00025	$+35 \pm 39$
	194	5887.82045 ± 0.00035	$+18 \pm 44$
	199	5895.68667 ± 0.00029	-5 ± 42
	206	5906.69953 ± 0.00041	-19 ± 50
	213	5917.71279 ± 0.00019	-1 ± 38
	229	5939.73781 ± 0.00030	-92 ± 45
	WASP-72 b	0	5583.6573 ± 0.0031
125		5860.7469 ± 0.0041	$+0.8 \pm 7.8$
139		5891.7832 ± 0.0027	$+3.9 \pm 6.3$
143		5900.6465 ± 0.0030	-0.9 ± 6.6

Table 7. Transit timings and TTVs ($O - C$ = observed minus computed timing) derived from the MCMC global analyses of the WASP-64 b and WASP-72 b transits.

show transits of very low-amplitude ($< 0.4\%$) in the WASP data. For WASP-64, the reason is not the intrinsic size contrast with the host star but the dilution of the signal by a close-by spectroscopic binary that could be dynamically bound to WASP-64 (Sec. 3.1).

Fig. 12 shows the position of both planets in a mass-radius diagram for a mass range from 1 to $2 M_{Jup}$. WASP-64 b has rather standard physical dimensions. Its measured radius of $1.27 \pm 0.04 R_{Jup}$ agrees well with the value of $1.19 \pm 0.11 R_{Jup}$ predicted by the equation derived by Enoch et al. (2012) from a sample of 71 transiting planets with a mass between 0.5 and $2 M_{Jup}$ and relating planets' sizes to their equilibrium temperatures and semi-major axes. On the contrary, WASP-72 b appears to be a possible outlier, its measured radius of $1.01^{+0.12}_{-0.08} R_{Jup}$ being marginally smaller than the value predicted by Enoch et al's empirical relation, $1.19 \pm 0.11 R_{Jup}$. Its density of $1.36 \pm 0.37 \rho_{Jup}$ is indeed surprisingly large considering its extreme irradiation ($\sim 4 \times 10^9 \text{ erg s}^{-1} \text{ cm}^{-2}$), indicating a possible enrichment of heavy elements. A comparison of WASP-72 b's radius with the theoretical planetary radii computed by Fortney et al. (2007) suggests indeed a very massive core ($> 50 M_{\oplus}$) for the planet that it will be important to confirm with future observations. Considering the solar metallicity of the host star and the difficulty of planet formation models to predict such dense giant planets (Mordasini et al. 2009), this could indicate a possible past heavy elements enrichment through one or several giant impacts phases (Ikoma et al. 2006), or through a significant loss of light elements by atmospheric evaporation (Lammer et al. 2009). Another possibility, of observational origin, is the dilution of the transit depth by the light of a second star. Still, the non-detection of any sign of a second stellar spectrum in our spectroscopic analysis (Sec. 3.1) advocates against this hypothesis.

While the non-detection of lithium in the spectra and the results of our stellar evolution modeling favor an age of several Gy for WASP-64, its measured $v \sin i_*$ of $3.4 \pm 0.8 \text{ km s}^{-1}$ leads to a much younger system under the gyrochronology relation

of Barnes (2007). Assuming that our $v \sin i_*$ measurement is not affected by a systematic error, this discrepancy strengthens the observation that stars hosting a hot Jupiter tend to rotate faster (Pont 2009), suggesting a significant tidal effect of close-in gas giants on their stars.

As described in Sec. 3.2, we have adopted the circular orbital models for both planets, basing on their larger marginal likelihoods. To assess the validity of this choice on a theoretical basis, we integrated the future orbital evolution of both systems through the low-eccentricity tidal model presented by Jackson et al. (2008), assuming as starting eccentricity the 95% upper limits derived in our MCMC analysis (0.132 for WASP-64 and 0.055 for WASP-72) and assuming mean values of 10^7 and 10^5 for, respectively, the stellar and planetary tidal dissipation parameters Q'_* and Q'_p (Goldreich & Soter, 1966). These integrations resulted in circularization times (defined as the time needed to reach $e < 0.001$) of 4 and 55 Myr for, respectively, WASP-64 b and WASP-72 b. These times are much shorter than the estimated age of the systems, strengthening our selection of the circular orbital solutions. It is worth mentioning that both systems are tidally unstable, as most of the hot Jupiter systems (Levrard et al. 2009), the times remaining for the planets to reach their Roche limits being respectively 0.9 Gy (WASP-64 b) and 0.6 Gy (WASP-72 b) under the assumed tidal dissipation parameters.

The new transiting systems reported here represent both two interesting targets for follow-up observations. Thanks to its extreme irradiation and its moderately large planet-to-star size ratio, WASP-64 b is a good target for near-infrared occultation (spectro-)photometry programs able to probe its day-side spectral energy distribution. Assuming a null albedo for the planet and blackbody spectra for both the planet and the host star, we computed occultation depths of 650-1550 ppm in K -band, 1500-2750 ppm at $3.6 \mu\text{m}$ and 2050-3350 ppm at $4.5 \mu\text{m}$, the lower and upper limits corresponding, respectively, to a uniform redistribution of the stellar radiation to both planetary hemispheres and to a direct reemission of the dayside hemisphere. Precise measurement of such occultation depths is definitely within the reach of several ground-based and space-based facilities (e.g. Gillon et al. 2012). For ground-based programs, the situation is made easier by the presence of a bright ($K = 9.8$) comparison star at only $28''$ from the target (Fig. 2). For WASP-72, atmospheric measurements are certainly more challenging considering the smaller planet-to-star size ratio. Here, the first follow-up actions should certainly be to confirm the large density of the planet through high-precision transit photometry and complementary analysis, and to gather more RVs to confirm the trend marginally detected in our analysis.

Acknowledgements. WASP-South is hosted by the South African Astronomical Observatory and we are grateful for their ongoing support and assistance. Funding for WASP comes from consortium universities and from UK's Science and Technology Facilities Council. TRAPPIST is a project funded by the Belgian Fund for Scientific Research (Fond National de la Recherche Scientifique, F.R.S-FNRS) under grant FRFC 2.5.594.09.F, with the participation of the Swiss National Science Foundation (SNF). M. Gillon and E. Jehin are FNRS Research Associates.

References

- Baranne A., Queloz D., Mayor M., et al., 1996, *A&AS*, 119, 373
- Barnes, S. A. 2007, *ApJ*, 669, 1167
- Bruntt, H., Deleuil, M., Fridlund, M., et al. 2010a, *A&A*, 519, A51
- Bruntt, H., Bedding, T. R., Quirion, P.-O., et al. 2010b, *MNRAS*, 405, 1907
- Claret A., 2000, *A&A*, 363, 1081
- Claret A., 2004, *A&A*, 428, 1001
- Collier-Cameron, A., Pollacco, D., Street, R. A., et al. 2006, *MNRAS*, 373, 799

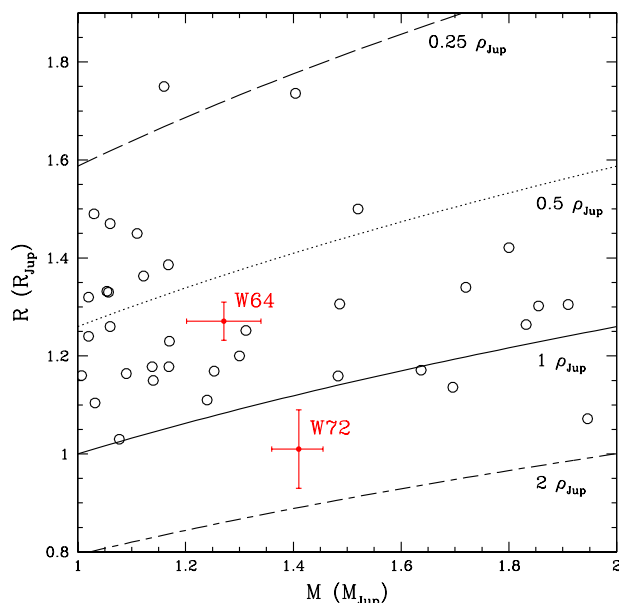


Fig. 12. Mass–radius diagram for the transiting planets with masses ranging from 1 to $2 M_{\text{Jup}}$. WASP-64 b and WASP-72 b are shown as red square symbols, while the other planets are shown as open circles without their error bars for the sake of clarity. Different iso-density lines are also shown.

- Collier-Cameron, A., Wilson, D. M., West, R. G., et al. 2007, *MNRAS*, 380, 1230
- Enoch, B., Collier-Cameron, A., Parley, N. R., Hebb, L. 2010 *A&A*, 516, A33
- Enoch, B., Collier-Cameron, A. & Horne, K. 2012, *A&A*, 540, A99
- Fortney J. J., Marley M. S., Barnes J. W. 2007, *ApJ*, 659, 1661
- Gelman A., Rubin D., 1992, *Statistical Science*, 7, 457
- Gillon, M., Smalley, B., Hebb, L., et al. 2009a, *A&A*, 496, 259
- Gillon M., Demory B.-O., Triaud A. H. M. J., et al., 2009b, *A&A*, 506, 359
- Gillon, M., Doyle, A. P., Lendl, M., et al. 2011, *A&A*, 533, A88
- Gillon, M., Jehin, E., Magain, P., et al. 2011, *Detection and Dynamics of Transiting Exoplanets*, Proceedings of OHP Colloquium (23-27 August 2010), eds. F. Bouchy, R. F. Diaz & C. Moutou, Platypus Press, 06002
- Gillon M., Triaud A. H. M. J., Fortney J. J., et al. 2012, *A&A*, 542, 4
- Goldreich, O. & Soter, S. 1966, *Icarus*, 5, 375
- Gray, D. F. 2008, *The observation and analysis of stellar photospheres*, 3rd Edition (Cambridge University Press), p. 507
- Hellier, C., Anderson, D. R., Collier-Cameron, A., et al. 2011, *Detection and Dynamics of Transiting Exoplanets*, Proceedings of OHP Colloquium (23-27 August 2010), eds. F. Bouchy, R. F. Diaz & C. Moutou, Platypus Press, 01004
- Holman M. J., Winn J. N., Latham D. W., et al., 2006, *ApJ*, 652, 1715
- Ikoma, M., Guillot, T., Genda, H., et al. 2006, *ApJ*, 650, 1150
- Jackson, D., Greenberg, R., & Barnes, R. 2008, *ApJ*, 678, 1396
- Jehin, E., Gillon, M., Queloz, D., et al. 2011, *The Messenger*, 145, 2
- Lammer, H., Odert, P., Leitzinger, M., et al. 2009, *A&A*, 506, 399
- Lendl, M., Anderson, D. R., Collier-Cameron, A., et al. 2012, *A&A*, 544, A72
- Levrard, B., Winisdoerffer, C. & Chabrier, G. 2009, *ApJL*, 692, 9
- Mandel K., Agol E., 2002, *ApJ*, 580, 181
- Magain P., 1984, *A&A*, 134, 189
- Maxted, P. F. L., Anderson, D. R., Collier Cameron, A., et al. 2011, *PASP*, 123, 547
- Mordasini, C., Alibert, Y., Benz, W., & Naef, D. 2009, *A&A*, 501, 1161
- Pollacco, D. L., Skillen, I., Collier Cameron, A., et al. 2006, *PASP*, 118, 1407
- Pont, F. 2009, *MNRAS*, 396, 1789
- Queloz D., Henry G. W., Sivan J. P., et al., 2001, *A&A*, 379, 279
- Roeser, S., Demleitner, M., & Schilbach, E. 2010, *AJ*, 139, 2440
- Schwarz, G. E. 1978, *Annals of Statistics*, 6, 461
- Scuflaire R., Théado S., Montalbán J., et al. 2008, *APSS*, 316, 149
- Sestito, P. & Randich, S. 2005, *A&A*, 442, 615
- Southworth, J., 2011, *MNRAS*, 417, 2166
- Stetson, P. B. 1987, *PASP*, 99, 111
- Torres, G., Andersen, J. & Giménez, A. 2010, *A&A Rev.*, 18, 67

<i>Free parameters</i>	$e \geq 0$	$e = 0$ (adopted)
Planet/star area ratio $(R_p/R_*)^2$ [%]	1.524 ± 0.025	1.522 ± 0.025
$b' = a \cos i_p/R_*$ [R_*]	$0.321^{+0.046}_{-0.065}$	$0.322^{+0.048}_{-0.068}$
Transit width W [d]	0.10005 ± 0.00047	0.09999 ± 0.00046
$T_0 - 2450000$ [HJD_{TDB}]	5582.60171 ± 0.00026	5582.60169 ± 0.00027
Orbital period P [d]	1.5732918 ± 0.000015	1.5732918 ± 0.000015
RV K_2 [$\text{m s}^{-1} \text{d}^{1/3}$]	248 ± 14	257 ± 11
RV γ [km s^{-1}]	33.191 ± 0.010	33.1854 ± 0.0057
$\sqrt{e} \cos \omega$	$0.083^{+0.081}_{-0.088}$	0 (fixed)
$\sqrt{e} \sin \omega$	-0.10 ± 0.15	0 (fixed)
$c1_V$	1.167 ± 0.058	1.168 ± 0.058
$c2_V$	0.017 ± 0.056	0.016 ± 0.061
$c1_{Gunn-r}$	0.983 ± 0.050	0.985 ± 0.050
$c2_{Gunn-r}$	-0.121 ± 0.044	-0.122 ± 0.045
$c1_{BB}$	1.040 ± 0.045	1.041 ± 0.045
$c2_{BB}$	-0.129 ± 0.053	-0.125 ± 0.051
$c1_{I+z}$	0.859 ± 0.053	0.856 ± 0.053
$c2_{I+z}$	-0.206 ± 0.041	-0.208 ± 0.0241
<i>Deduced stellar parameters</i>		
Density ρ_* [ρ_\odot]	$0.90^{+0.16}_{-0.09}$	$0.849^{+0.053}_{-0.044}$
Surface gravity $\log g_*$ [cgs]	$4.406^{+0.044}_{-0.029}$	4.392 ± 0.016
Mass M_* [M_\odot]	$0.993^{+0.034}_{-0.037}$	1.004 ± 0.028
Radius R_* [R_\odot]	$1.036^{+0.046}_{-0.065}$	1.058 ± 0.025
Luminosity L_* [L_\odot]	0.90 ± 0.15	0.95 ± 0.13
$u1_V$	0.470 ± 0.033	0.470 ± 0.035
$u2_V$	0.226 ± 0.027	0.227 ± 0.028
$u1_{Gunn-r}$	0.369 ± 0.027	0.370 ± 0.027
$u2_{Gunn-r}$	0.245 ± 0.020	0.246 ± 0.020
$u1_{BB}$	0.391 ± 0.025	0.392 ± 0.025
$u2_{BB}$	0.259 ± 0.023	0.259 ± 0.022
$u1_{I+z}$	0.302 ± 0.028	0.301 ± 0.028
$u2_{I+z}$	0.255 ± 0.017	0.255 ± 0.018
<i>Deduced planet parameters</i>		
RV K [m s^{-1}]	214 ± 13	221 ± 11
R_p/R_*	0.1234 ± 0.0011	0.1234 ± 0.0011
b_{I_r} [R_*]	$0.313^{+0.049}_{-0.064}$	$0.322^{+0.048}_{-0.068}$
b_{oc} [R_*]	$0.296^{+0.059}_{-0.070}$	$0.322^{+0.048}_{-0.068}$
$T_{oc} - 2450000$ [HJD_{TDB}]	$5583.403^{+0.026}_{-0.024}$	5583.38834 ± 0.00029
Orbital semi-major axis a [AU]	$0.02640^{+0.00030}_{-0.00033}$	0.02648 ± 0.00024
a/R_*	$5.49^{+0.31}_{-0.19}$	$5.39^{+0.11}_{-0.09}$
Orbital inclination i_p [deg]	$86.69^{+0.79}_{-0.66}$	$86.57^{+0.80}_{-0.60}$
Orbital eccentricity e	$0.035^{+0.039}_{-0.025}$	0 (fixed)
	< 0.132 (95%)	-
Argument of periastron ω [deg]	308^{+80}_{-36}	-
Equilibrium temperature T_{eq} [K] ^a	1672^{+59}_{-63}	1689 ± 49
Density ρ_p [ρ_{Jup}]	$0.64^{+0.12}_{-0.08}$	$0.619^{+0.064}_{-0.052}$
Surface gravity $\log g_p$ [cgs]	$3.294^{+0.049}_{-0.043}$	3.292 ± 0.030
Mass M_p [M_{Jup}]	1.217 ± 0.083	1.271 ± 0.068
Radius R_p [R_{Jup}]	$1.244^{+0.062}_{-0.080}$	1.271 ± 0.039

Table 5. Median and 1- σ limits of the marginalized posterior distributions obtained for the WASP-64 system parameters as derived from our MCMC analysis. ^aAssuming a null Bond albedo ($A_B=0$) and isotropic reradiation ($f=1/4$).

<i>Free parameters</i>	$e \geq 0$	$e = 0$ (adopted)
Planet/star area ratio $(R_p/R_*)^2$ [%]	0.367 ± 0.031	0.367 ± 0.030
$b' = a \cos i_p/R_*$ [R_*]	$0.24^{+0.18}_{-0.15}$	$0.24^{+0.18}_{-0.15}$
Transit width W [d]	0.1567 ± 0.0052	$0.1565^{+0.0057}_{-0.0051}$
$T_0 - 2450000$ [HJD_{TDB}]	5583.6557 ± 0.0032	5583.6557 ± 0.0031
Orbital period P [d]	2.216727 ± 0.000015	2.216726 ± 0.000015
RV K_2 [$\text{m s}^{-1} \text{d}^{1/3}$]	237.0 ± 5.5	236.4 ± 5.4
RV γ [km s^{-1}]	35.923 ± 0.015	35.919 ± 0.013
RV slope [$\text{m s}^{-1} \text{y}^{-1}$]	-43 ± 19	-38 ± 17
$\sqrt{e} \cos \omega$	-0.029 ± 0.068	0 (fixed)
$\sqrt{e} \sin \omega$	-0.07 ± 0.11	0 (fixed)
$c1_{Gunn-r}$	0.940 ± 0.026	0.940 ± 0.026
$c2_{Gunn-r}$	-0.317 ± 0.016	-0.316 ± 0.016
$c1_{BB}$	0.822 ± 0.078	0.828 ± 0.076
$c2_{BB}$	-0.352 ± 0.044	-0.349 ± 0.043
$c1_{I+z}$	0.700 ± 0.041	0.702 ± 0.042
$c2_{I+z}$	-0.387 ± 0.028	-0.386 ± 0.029
<i>Deduced stellar parameters</i>		
Density ρ_* [ρ_\odot]	$0.253^{+0.044}_{-0.058}$	$0.265^{+0.044}_{-0.057}$
Surface gravity $\log g_*$ [cgs]	$4.082^{+0.045}_{-0.073}$	$4.095^{+0.042}_{-0.066}$
Mass M_* [M_\odot]	$1.335^{+0.044}_{-0.034}$	$1.327^{+0.043}_{-0.035}$
Radius R_* [R_\odot]	$1.74^{+0.18}_{-0.10}$	$1.71^{+0.16}_{-0.09}$
Luminosity L_* [L_\odot]	$4.17^{+0.94}_{-0.57}$	$4.02^{+0.85}_{-0.52}$
$u1_{Gunn-r}$	0.313 ± 0.014	0.313 ± 0.014
$u2_{Gunn-r}$	0.3148 ± 0.0061	0.3142 ± 0.0065
$u1_{BB}$	0.258 ± 0.041	0.261 ± 0.041
$u2_{BB}$	0.305 ± 0.014	0.305 ± 0.014
$u1_{I+z}$	0.202 ± 0.023	0.204 ± 0.023
$u2_{I+z}$	0.295 ± 0.013	0.295 ± 0.013
<i>Deduced planet parameters</i>		
RV K [m s^{-1}]	181.9 ± 4.9	181.3 ± 4.7
R_p/R_*	0.0606 ± 0.0028	0.0606 ± 0.0030
b_{lr} [R_*]	$0.25^{+0.22}_{-0.17}$	$0.24^{+0.18}_{-0.15}$
b_{oc} [R_*]	$0.24^{+0.22}_{-0.17}$	$0.24^{+0.18}_{-0.15}$
$T_{oc} - 2450000$ [HJD_{TDB}]	5584.760 ± 0.021	5584.7640 ± 0.0031
Orbital semi-major axis a [AU]	$0.03662^{+0.00040}_{-0.00031}$	$0.03655^{+0.00039}_{-0.00032}$
a/R_*	$4.53^{+0.25}_{-0.38}$	$4.59^{+0.24}_{-0.39}$
Orbital inclination i_p [deg]	$86.7^{+2.1}_{-3.3}$	$86.8^{+2.0}_{-3.1}$
Orbital eccentricity e	$0.015^{+0.018}_{-0.011}$	0 (fixed)
	< 0.055 (95%)	-
Argument of periastron ω [deg]	111^{+88}_{-51}	-
Equilibrium temperature T_{eq} [K] ^a	2080^{+97}_{-66}	2064^{+90}_{-62}
Density ρ_p [ρ_{Jup}]	1.30 ± 0.36	1.36 ± 0.37
Surface gravity $\log g_p$ [cgs]	$3.521^{+0.070}_{-0.088}$	$3.534^{+0.070}_{-0.088}$
Mass M_p [M_{Jup}]	$1.421^{+0.054}_{-0.047}$	$1.410^{+0.050}_{-0.045}$
Radius R_p [R_{Jup}]	$1.03^{+0.12}_{-0.08}$	$1.01^{+0.12}_{-0.08}$

Table 6. Median and 1- σ limits of the marginalized posterior distributions obtained for the WASP-72 system parameters as derived from our MCMC analysis. ^aAssuming a null Bond albedo ($A_B=0$) and isotropic reradiation ($f=1/4$).